

## Chapter 2

# Ion Acceleration I: Efficient Heavy Ion Acceleration by ESA

### 2.1 Introduction

Monoenergetic ion beams play essential roles in many important applications such as fast ignition fusion, cancer therapy, and other applications [1]. The new accelerating method, laser ion acceleration, attracts more and more attention nowadays since the acceleration gradient is at least four magnitudes higher than that of conventional methods. A number of novel mechanisms have been proposed for accelerating protons or heavier ions to high energies using the recently available high-intensity short-pulse lasers. With target-normal sheath acceleration, protons up to 58 MeV have been obtained with  $3 \times 10^{20}$  W/cm<sup>2</sup> lasers [2]. With microstructured targets, quasi-monoenergetic proton or ion bunches with energy spread of about 20 % have been produced [3, 4]. Other promising schemes include shock acceleration at the front of the foil [5–9], direct laser-pressure acceleration [10, 11], and acceleration by plasma wake [12].

Despite these improvements, acceleration of heavy ions by laser plasma interaction is still a challenge [13] because of certain physical limits. Heavy ions cannot be accelerated as efficiently as protons because of their lower charge-mass ratios. The electric force per unit mass on them is smaller. Accordingly, the target should be free of protons that would be preferentially accelerated [14], which puts strict requirements on experimental setups.

In this chapter, an efficient and simple method of heavy ion acceleration is proposed with the mechanism of electrostatic shock acceleration (ESA), where circularly polarized (CP) laser is used as the driver. As discussed in Chap. 1, the ponderomotive force of a CP laser does not contain an oscillating component, thus electrons in target are less heated than that for other polarizations. They are pushed forward and compressed by the light pressure, forming an intense self-consistent space-charge field that can accelerate the ions [15]. When the laser pulse is flat-topped, the perturbed system can propagate as an electrostatic shock. In the latter, the ions are mostly trapped and reflected forward at a nearly constant velocity, leading to the formation of a monoenergetic ion beam and a flat-top structure in the ion phase space [16]. In ESA, according to the scaling law of

Eq. (1.60), one can reduce the target density to obtain heavy ion bunches with higher energy. However, the target density must be above the relativistic critical value, so that the target remains opaque to the laser and the resulting space-charge field is sufficiently high to trap local ions [17].

Things become interesting when a compound target is used. It will be shown in the following simulations that, when the target consists of two ion species, both the heavy and light ions will be trapped and accelerated to the same velocity. A most important feature is that the common velocity is higher than when the target consists of only heavy ions, having the other parameters unchanged. This suggests a simple way to raise the energy of heavy ions: adding protons to the heavy ion target.

It should be noted that using compound or multilayer targets is not new in laser ion acceleration [3, 4, 12, 18–20]. But the heavy ions were more likely to be used as a background to increase the gradient of the space-charge field for proton acceleration. The corresponding laser pulses were usually linearly polarized. Furthermore, the resulting heavy ions from existing compound targets were not monoenergetic. To improve the quality of the accelerated heavy ions, in this chapter a sandwich target structure is employed. The latter consists of a thin compound ion layer between two light ion layers. In 3D, the target is micro-structured to yield ion beams of good quality. Simulation results show that at a laser intensity of  $5 \times 10^{19} \text{ Wcm}^{-2}$  a carbon ion beam with energy divergence about 5 % at the longitudinal kinetic energy of  $E_x \sim 58 \text{ MeV}$ , with a total carbon ion number of about  $3.36 \times 10^8$  (a total charge of  $3.23 \times 10^{-10} \text{ C}$ ) can be obtained.

## 2.2 CP Laser Interacting with Multispecies Target

First, a one-dimensional simulation is performed to observe the interaction between a relativistic CP laser pulse and a compound target, using the code VORPAL [21]. The light ion species is proton with charge and mass number of  $Z_1 = A_1 = 1$  while the heavy one is carbon with  $Z_2 = 6$  and  $A_2 = 12$ . A CP laser pulse with wavelength of  $\lambda_0 = 1 \mu\text{m}$  irradiates the target from the left. The laser amplitude rises from zero to  $a_L = 2$  in  $6T_0$ , where  $T_0$  is the laser period, and then remains constant for  $200T_0$ . The simulation box is  $101\lambda_0$  long in the  $x$  direction, and the cold target initially occupies the region between  $x = 80.5\lambda_0$  and  $x = 82.5\lambda_0$ . The total electron density of the target is  $n_e = 5n_c$ , and the densities of the two ion species are given by  $n_{e1} = n_{e2} = 0.5n_e$ .

Figure 2.1a shows the phase space of the light and heavy ions, together with the electric field distribution. The presence of the collisionless electrostatic shock structure can be clearly seen. Almost all of both types of ions are trapped (reflected) by the electrostatic field, which is created through the laser-compressed electrons. In the region of the charge separating field, light ions seem to obtain prior acceleration and move ahead of heavy ions. However, all reflected ions move

forward together when they leave the high-field region eventually. The light and heavy ions do not have different final velocities.

This interesting feature indicates that all ions and the accelerating field belong to the same self-consistent electrostatic shock system, whose speed is self-consistently determined by the laser plasma parameters, including the charge and mass of both ion species. Since the carbon mass is 12 times that of hydrogen, the energy per carbon ion is about 12 times that of protons, as can be clearly seen in Fig. 2.1b.

### 2.3 Analytical Modeling

The above simulation shows that the heavy and light ions are mostly trapped and accelerated to the same velocity. Assuming all the ions are accelerated, from momentum and energy conservation one obtains

$$\frac{I}{c} = -\eta \frac{I}{c} + \left( n_{e1} \frac{A_1}{Z_1} + n_{e2} \frac{A_2}{Z_2} \right) m_p v_i v_a, \quad (2.1)$$

$$I = \eta I + \left( n_{e1} \frac{A_1}{Z_1} + n_{e2} \frac{A_2}{Z_2} \right) \frac{m_p v_i^2}{2} v_a, \quad (2.2)$$

where  $I$  and  $\eta$  are the intensity and reflectivity of the laser pulse,  $m_p$  is proton mass,  $v_i$  and  $v_a$  are the velocities of the reflected ions and the shock, respectively,  $Z$  and  $A$  are ion charge and mass number, and  $n_{e1} \equiv Z_1 n_{i1}$ ,  $n_{i1}$  and  $n_{e2} \equiv Z_2 n_{i2}$ ,  $n_{i2}$  are the corresponding electron and ion densities of each species, respectively. The subscripts 1 and 2 denote the light and heavy ion species. Since the ions are reflected by the shock, the final velocity is about  $v_i \approx 2v_a$ , thus Eqs. (2.1) and (2.2) give

$$\frac{v_i}{c} \approx 2 \sqrt{\frac{n_c}{n_{e1} A_1 / Z_1 + n_{e2} A_2 / Z_2}} \sqrt{\frac{m_e}{m_p} a_L}, \quad (2.3)$$

where  $n_c$  is the critical plasma density,  $m_e$  the electron mass,  $c$  the light speed,  $a_L = eE_L / m_e \omega_L c$  the dimensionless laser electric field,  $e$  the elementary charge, and  $E_L$  and  $\omega_L$  are the electric field amplitude and frequency of the laser. For a single-ion target, Eq. (2.3) reduces to Eq. (1.60).

To express it more clearly, Eq. (2.3) is rewritten in terms of the ratios  $\alpha = n_{e1} / n_{e2}$  and  $\beta = (Z_1 / A_1) / (Z_2 / A_2)$  as

$$v_i / c \approx 2 \sqrt{1 + \frac{\alpha(\beta - 1)}{\alpha + \beta}} \sqrt{\frac{Z_2}{A_2} \frac{m_e}{m_p} \frac{n_c}{n_e} a_L}, \quad (2.4)$$

so that the effects of density ratio and different species on the acceleration efficiency become more transparent. For comparison, a series of simulations are carried out for various combinations of  $\alpha$  and  $\beta$  values. The other conditions are

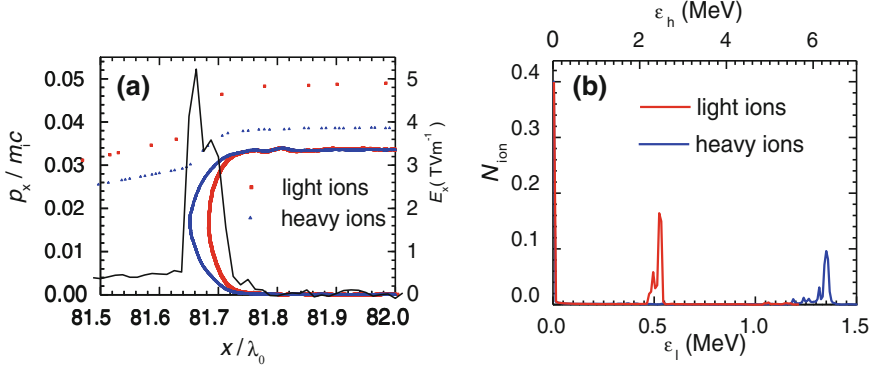


**Fig. 2.1** **a** Phase space of the light (red-dotted) and heavy ions (blue-dotted) and the electric field distribution (black solid) of the collisionless electrostatic shock at  $t = 150 T_0$  for  $a_L = 2$ ,  $n_e = 5n_c$ , and  $d = 2 \lambda_0$ . **b** The energy spectrum of the light and heavy ions.  $\epsilon_l$  and  $\epsilon_h$  are the corresponding longitudinal kinetic energies, and  $N_{\text{ion}}$  is the normalized ion number. The compound target is a mixture of hydrogen (light) and carbon (heavy) with  $n_{e1} = n_{e2} = 0.5n_e$

the same as in Fig. 2.1. The results are shown in Fig. 2.2, where an excellent agreement appears between the simulation and Eq. (2.4). Both simulations and analysis prove that the important feature exists for a very wide parameter range in shock acceleration. In Fig. 2.2a, one finds that the collective velocity in the compound target case is higher than that in the heavy ion only target case. That is to say, the energy of heavy ions can be easily increased by mixing with some light ions.

In order to improve heavy ion acceleration efficiently, Fig. 2.2a shows that its concentration must be much lower than that of proton. On the other hand, since the common velocity increases quickly with the density ratio at first and then slowly saturates to the maximum, the concentration of the heavy ions need not be reduced very much to achieve significant energy increment. This point is important to guarantee that the number of energetic heavy ions per bunch will not be too small. For example, for  $n_{e1}/n_{e2} = 9$ , or a carbon ion density of  $10^{20} \text{ cm}^{-3}$ , the velocity is  $0.039 c$ , which is increased by 34.5 % with respect to the pure heavy ion target case, or 81 % by kinetic energy. It is close to the predicted maximum value of 41.5 % by Eq. (2.4). One should also note that the increasing rate of heavy ion energy does not depend on the other laser and target parameters as long as the shock acceleration mechanism dominates.

The results here stem from a self-consistent phase-mixing effect in the collisionless electrostatic shock. The local ions (electrons) are reflected, or accelerated, forward (backward) by the electrostatic space-charge field driven by the laser pulse. The light ions (with larger charge-mass ratio) tend to move faster than heavy ions. The faster (slower) ions will be pulled back (pushed forward), resulting in a redistribution of the space-charge-field. In such a manner, heavy ions experience stronger accelerating field while light ions less. Finally, the entire system moves

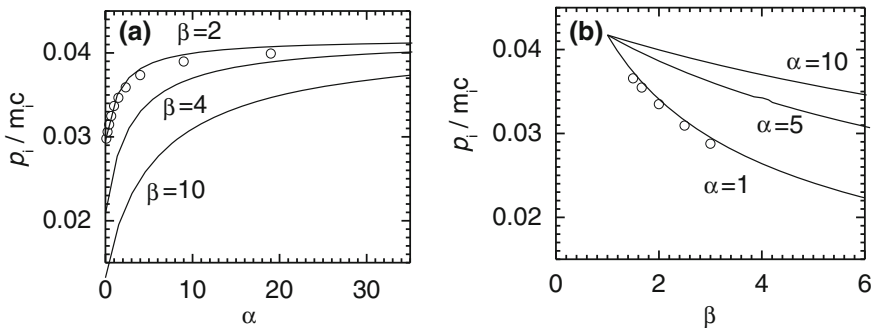


**Fig. 2.2** Reflected heavy ion momentum *versus* **a**  $\alpha$  and **b**  $\beta$  from simulations (circles) and Eq. (2.4) (solid line) at  $t = 150 T_0$ . The other parameters are the same as in Fig. 2.1

together at a common speed. It seems that heavy ions are drawn by light ions indirectly, hence the light ions are slightly ahead of the heavy ions and a tiny valley exists in the electrostatic field distribution between the two reflected ion fronts in Fig. 2.1a. The circularly polarized laser pulse maintains the electrostatic field, whereas the response of the electron-ion plasma is another key of this interesting phenomenon. It should be mentioned that the higher the shock speed, the longer the time for picking up all heavy ions. PIC simulations also find that more complex multispecies targets (such as that with three species) exhibit similar phenomenon.

## 2.4 Generating Monoenergetic Heavy Ion Beam

In the above consideration, the laser pulse is flat-topped and the accelerated ions are monoenergetic. In most practical cases lasers are roughly Gaussian, so that according to Eq. (2.3), the accelerated ions may not be monoenergetic any more. The energy spread should be improved to fulfill the requirements of various applications.

### 2.4.1 “Sandwich” Target in One-Dimensional Simulation

To overcome the difficulty, a simple and effective method is presented. A sandwich target with a thin compound layer between two light ion layers is used, as seen in Fig. 2.3a. By this target structure, the beginning of the laser pulse would interact with the light ion layer in the front; then the following part with much smaller duration irradiates the thin compound layer, leaving the rest to the second light ion layer at the back. As the inside compound layer is very thin, its interacting

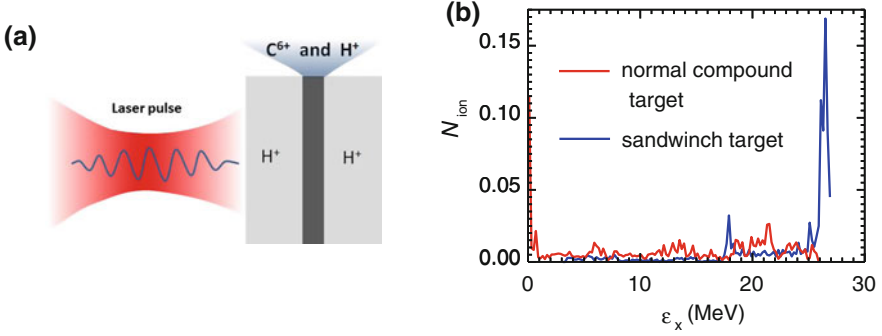


**Fig. 2.3** Sandwich target scheme (a) and energy spectrum of normal compound target (*red solid*) and sandwich target (*blue solid*) (b) at  $t = 240 T_0$  for a Gaussian laser pulse with peak amplitude  $a_L = 4$  and duration of  $220 T_0$ . The inside central compound layer (hydrogen and carbon) is  $0.2 \lambda_0$  thick with  $\alpha = 1$  and the outer two light ion layers (hydrogen) are both  $0.9 \lambda_0$  thick

time with partial laser pulse is short enough that the laser intensity keeps almost constant, which eventually leads to a more monoenergetic heavy ion bunch.

Here position and thickness of the thin layer have great influence on the beam quality. Taking Gaussian laser pulses for example, the intensity peaks in the center. It is better to place the compound layer in the right position of the target to make it interact with only the central part of the laser pulse, and thus ions would gain peak energy. Moreover, the energy spread may be manipulated by controlling the interacting time, which could be realized through the variation of the layer thickness. In a word, both the peak energy and the energy spread of the heavy ion beam can be regulated. A single thin compound foil cannot work like this because it might be destroyed by pre-pulse of the laser. It is also more convenient to produce this sandwich target than a single thin compound foil. The two light ion layers are attached to make the two ion species convenient to be separated in succeeding treatments.

For 1D simulations, the cold sandwich target electron density is  $5n_c$  and the target is located from  $x = 80.5\lambda_0$  to  $x = 82.5\lambda_0$ , while length of the simulation box is  $101\lambda_0$ . The central thin layer is a mixture of hydrogen and carbon ( $\beta = 2$ ) with electron density ratio of  $\alpha = 1$ . Its thickness is  $0.2\lambda_0$  and both the front and back hydrogen layers are  $0.9\lambda_0$ . The peak amplitude of the Gaussian laser pulse is  $a_L = 4$  and its duration is  $220 T_0$ . Comparison of ion energy spectrum with normal compound target is shown in Fig. 2.3b. All figures are taken at  $t = 240 T_0$  as the interaction is just over. An obvious improvement can be seen in the sandwich target way, by which carbon ions are almost around peak energy 26 MeV while the other is nearly averagely distributed. The parameters chosen here are to guarantee that the compound layer interacts only with the center part of Gaussian pulse in a short time, therefore heavy ions are well monoenergetic with peak energy. The peak energy is perfectly four times as in Fig. 2.1b according to the scaling law of Eq. (2.3), indicating that the acceleration scheme is well in operation.

### 2.4.2 Microstructured Target in Three-Dimensional Simulation

One may doubt the efficiency in practice because so far no 2D or 3D effects have been counted in. It has been confirmed by 2D PIC simulations in [15] that 2D effects do not have qualitatively influence on ion bunch formation, but it does affect energy and beam divergence of ion bunches. To weaken the negative effects, we reduced the transverse dimension of the inside thin compound layer. The target is microstructured with a compound microdot in it. Accordingly, a 3D PIC simulation by VORPAL is carried out. “1” and “2” denote hydrogen and carbon, respectively.

The simulation box is  $25\lambda_0 \times 120\lambda_0 \times 120\lambda_0$ . The microstructured target occupies a region of  $15\lambda_0 - 17\lambda_0$  ( $2\mu\text{m}$ ) in  $x$  (longitudinal) and  $-54\lambda_0 - 54\lambda_0$  ( $108\mu\text{m}$ ) in both  $y$  and  $z$  (transverse) with total electron density of  $5n_c$ . The inside microdot is mixed with hydrogen and carbon by  $\alpha = 1$ , occupying a region of  $15.4\lambda_0 - 15.435\lambda_0$  ( $35\text{nm}$ ) longitudinally and  $-2.4\lambda_0 - 2.4\lambda_0$  ( $4.8\mu\text{m}$ ) transversely. The rest of the target is made up of light ions. The Gaussian laser pulse with beam waist radius  $w_0 = 17\lambda_0$ , peak amplitude  $a_L = 6$  and a duration of  $40T_0$  propagates from the left. Figure 2.4a shows the proton (black) and carbon ion (red) distributions at  $t = 30T_0$  where ions in the outer part of the target are eliminated to display the inside structure. The proton density shows a Gaussian-like front due to the Gaussian profile of the transverse laser intensity. All carbon ions in the compound layer have been reflected, leading to a compact beam with very small dimension. From phase space and longitudinal kinetic energy spectrum at different moment in Fig. 2.4b and c, the following process is shown clearly: the compound microdot is initially irradiated by laser front; carbon ions are being accelerated by the electrostatic field; carbon ions are all trapped and reflected, and finally propagating stably. This exactly describes the motion of the heavy ion from  $t = 20T_0$  to  $t = 32T_0$ . In the end, aquasi-monoenergetic carbon ion bunch with peak energy of  $E_x \sim 58\text{MeV}$  and energy spread of about 5% is generated. The beam carries a total carbon ion number of about  $3.36 \times 10^8$  (that is, a total charge of  $3.23 \times 10^{-10}\text{C}$ ). Collimation of the obtained carbon ion bunch is pretty good as seen in Fig. 2.4d, with maximal divergence angle of  $\Delta\theta_{\max} \sim 6 \times 10^{-3}\pi$  rad.

The peak energy in Fig. 2.4c is about nine times as in Fig. 2.1b, verifying the scaling law again. One then concludes that 3D effect does not qualitatively impact acceleration mechanism either, and the proposed method turns out to be very effective. The transverse dimension of the microdot can be changed to control the energy divergence.

## 2.5 Summary and Discussion

In summary, a target with two ion species irradiated by a circularly polarized laser pulse is examined by PIC simulations. It is found that the two ion species are accelerated to the same velocity which is higher than in the case of the pure heavy

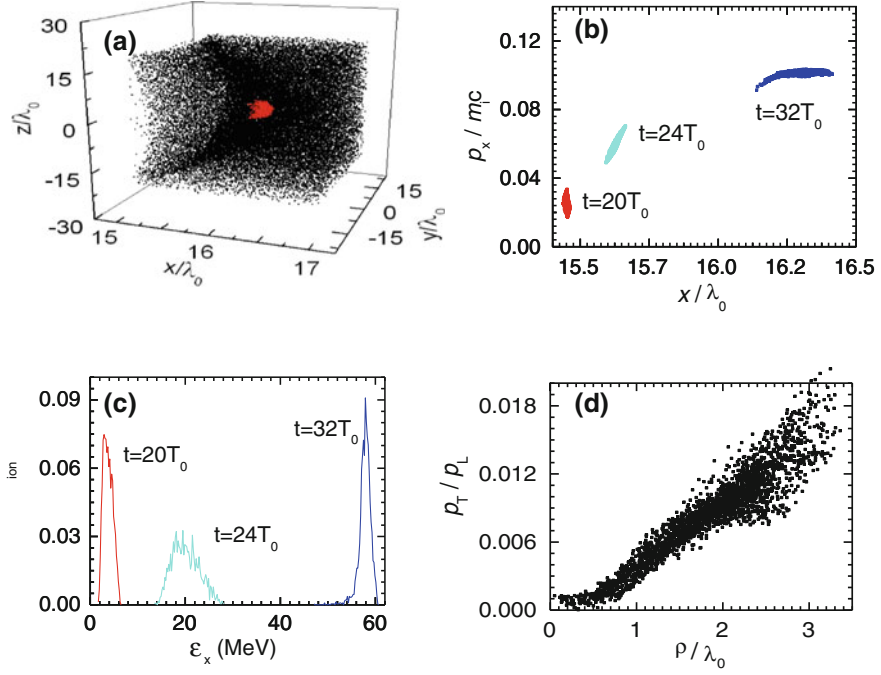


**Fig. 2.4** Spatial distributions of hydrogen (black dots) and carbon ions (red dots) at  $t = 30T_0$  (a); phase space (b) and energy spectrum (c) of heavy ions at different time and transverse distribution of  $p_L/p_T$  (d), where  $p_L = \gamma m_i v_{ix}$  and  $p_T = \gamma m_i (v_{iy}^2 + v_{iz}^2)^{1/2}$  are heavy ions' longitudinal and transverse momentum and  $\rho = (y^2 + z^2)^{1/2}$  is the distance from the target center

ion target. A simple model based on momentum and energy conservations is proposed and it describes the found effect very well. When the laser pulse is not uniform in space and time, a sandwich microstructured target with a compound microdot in it is proposed. The 3D PIC simulation suggests that a quasi-monoenergetic heavy ion bunch can be generated. This method is so effective and practical that the energy of the heavy ions can easily be raised by nearly 100 % (or higher for heavier ions) under the same laser conditions. The qualities of the heavy ion beam, including the energy and space divergence, are significantly improved by using the microstructured target.

As an estimate, the LULI laser system (wavelength  $\sim 1\mu\text{m}$ , intensity  $\sim 10^{19}\text{Wcm}^{-2}$ , focal aperture  $5 - 10\mu\text{m}$  and duration about 300 fs) should be able to generate a carbon beam with a peak energy of 12 MeV and a total carbon ion number of  $\sim 10^8$  while the energy divergence is still kept at 5 %. Moreover, the fraction of carbon ions in the target can be reduced such that a maximum accelerated energy of 18 MeV can be obtained.



## References

1. M. Roth et al, Phys. Rev. Lett. **86**, 436 (2001)
2. R.A. Snavely et al., Phys. Rev. Lett. **85**, 2945 (2000)
3. H. Schwoerer et al., Nature **439**, 445–448 (2006)
4. B.M. Hegelich et al., Nature **439**, 441–444 (2006)
5. L.O. Silva et al., Phys. Rev. Lett. **92**, 015002 (2004)
6. J. Denavit, Phys. Rev. Lett. **69**, 3052 (1992)
7. Y. Sentoku et al., Phys. Plasmas **10**, 2009 (2003)
8. A. Zhidkov et al., Phys. Rev. Lett. **89**, 215002 (2002)
9. E.d'Humières et al., Phys. Plasmas **12**, 062704 (2005)
10. B. Shen et al., Phys. Rev. E **64**, 056406 (2001)
11. T. Esirkepov et al., Phys. Rev. Lett. **92**, 175003 (2004)
12. B. Shen et al., Phys. Rev. E **70**, 036403(R) (2004)
13. M. Hegelich et al., Phys. Rev. Lett. **89**, 085002 (2002)
14. B.M. Hegelich et al., Phys. Plasmas **12**, 056314 (2005)
15. A. Macchi et al., Phys. Rev. Lett. **94**, 165003 (2005)
16. X. Zhang et al., Phys. Lett. A **369**, 339–344 (2007)
17. X. Zhang et al., Phys. Plasmas **14**, 123108 (2007)
18. A.P.L. Robinson et al., Phys. Rev. Lett. **96**, 035005 (2006)
19. M. Chen et al., Phys. Plasmas **14**, 113106 (2007)
20. T.Zh Esirkepov et al., Phys. Rev. Lett. **89**, 175003 (2002)
21. C. Nieter, J.R. Cary, J. Comp. Phys. **196**, 448 (2004)

<http://www.springer.com/978-3-642-54006-6>

Ion acceleration and extreme light field generation  
based on ultra-short and ultra-intense lasers

Ji, L.

2014, XII, 84 p. 46 illus., 16 illus. in color., Hardcover

ISBN: 978-3-642-54006-6